SCIENTIFIC PAPERS
OF THE UNIVERSITY OF PARDUBICE
Series A
Faculty of Chemical Technology
20 (2014)

EVALUATION OF STRUCTURAL AND CHARGE PROPERTIES OF POLYAMIDE NANOFILTRATION MEMBRANE

Cristina V. GHERASIM[1], Petr MIKULÁŠEK, Jaromíra CHÝLKOVÁ and Anna KREJČOVÁ
Institute of Environmental and Chemical Engineering,
The University of Pardubice, CZ–532 10 Pardubice

Received March 21, 2014

Nanofiltration (NF) is a highly efficient membrane separation process which has various environmental and industrial applications. Nanofiltration membranes are finely porous membranes with specific interesting features, their characterization being important for understanding of the NF processes and for their prediction for practical use. A polyamide thin-film composite NF membrane (AFC 80) was characterized in the present work by two different techniques: modelling of the rejection of uncharged solutes and modelling of the salt rejection. The interpretation of the data from uncharged solutes rejection experiments by using Donnan steric partitioning pore model (DSPM) allows to determine the structural characteristics of the AFC 80 membrane, i.e., effective pore radius (r_p), and thickness to porosity ratio ($\Delta x/A_k$). The experimental data for sodium chloride rejection were used to calculate the effective fixed charge density (ΦX) by means

[1] To whom correspondence should be addressed (Cristina-Veronica.Gherasim@upce.cz).

of an irreversible thermodynamics model (Spiegler–Kedem model) and of a charge model, namely Teorell–Meyer–Sievers (TMS) model. It was found that the membrane charge depends on the salt concentration in solution, this behaviour being attributed to ion adsorption on the membrane. The dependence of the charge density on NaCl concentration obeys a Freundlich isotherm equation.

Introduction

Nanofiltration (NF) is a relatively new pressure-driven membrane water treatment technique which has had more and more applications in environmental and industrial areas in the last years. This technique has separation characteristics between ultrafiltration (UF) and reverse osmosis (RO), and has also some important advantages such as: high rejection of divalent ions accompanied by lower rejection of monovalent ions, lower operating pressure, higher flux and lower energy consumption comparing with RO [1]. NF membranes have interesting properties which combine size and charge effects, namely very small pores (<1 nm), and they are positively or negatively charged, depending on their materials. Thus, NF membranes are able to retain neutral species with MW < 200-300 g mol^{-1}, and also to reject inorganic ions by a size exclusion mechanism combined with electrostatic interactions between the ions and the charges developed by dissociation of groups on the membrane active layer [2]. However, due to the fact that the separation mechanism of the NF membranes is very complex, it is not yet fully understood [1].

In order to explain and predict the separation properties of NF membranes, it is necessary to determine their structural and electrical properties. The structural properties are related to the pore size and membrane thickness, and the electrical properties refer to the sign and magnitude of the charge of the membrane active layer. The pore size and the charge determine the rejection of the solutes, and the membrane thickness determines the hydrodynamic resistance of the membrane and, therefore, the pressure which can withstand and the flux through the membrane [3]. Direct measurement of the structural properties by atomic force microscopy (AFM) is not very precise for NF membranes due to the fact that the pores are very small and also the images of the membrane surface cannot give information about the structure of the pore inside the membrane (tortuosity and shape) which actually determine the transport of the solutes through the NF membranes; also, the methods used for determination of the membrane charge density, i.e., electrokinetic measurements, measurements of membrane potential or determination of the ion-exchange capacity, can give mainly qualitative information [4]. A widely applied method to determine the membrane characteristics is by performing rejection experiments of uncharged solutes and salts, followed by using of models for calculation of pore size, effective thickness

to porosity ratio, and the membrane charge density.

Due to the fact that the separation mechanism of the NF membranes is very complex, numerous models were developed in order to describe in an appropriate way the flux and the retention of various species in NF. These models can be divided into several classes, namely: irreversible thermodynamics (IT) models, pore models, and non-porous (homogenous) models. The most frequently used models for determination of the NF membrane characteristics are pore models like Donnan steric partitioning pore model (DSPM) [5,6], the well known IT model developed by Spiegler and Kedem [7], steric hindrance pore model (SHP) [8], or more complex Donnan steric pore model & dielectric exclusion [9]. A rigorous approach for describing the electrical properties of the membranes and for determining the charge density of the NF membranes is the Teorell–Meyer–Sievers (TMS) model [8,10].

In the present work, the structural parameters, i.e., pore radius (r_p) and thicknesses to porosity ratio ($\Delta x/A_k$) of a thin-film composite polyamide NF membrane (AFC 80) are determined by rejection experiments of different uncharged solutes on the basis of DSPM model. The charge properties of the membrane top layer were investigated from rejection experiments of different concentrations of sodium chloride by means of Spiegler–Kedem (SK) and TMS models.

Theory

Concentration Polarization in Nanofiltration

By measuring the solute concentrations in feed (retentate) solution ($C_{i,f}$) and also in permeate solution ($C_{i,p}$) , the observed rejection is given by Eq. (1)

$$R_o = 1 - \frac{C_{i,p}}{C_{i,f}} \tag{1}$$

In NF processes, the pressure applied on the feed side of the membrane leads to a solvent flow through the membrane pores accompanied by a partial permeation of the solutes. Therefore, the solutes retained by the NF membrane are accumulated near the membrane surface, and the concentration of the solutes in the bulk of the feed ($C_{i,f}$) differs from their concentration in the near vicinity of the membrane surface ($C_{i,m}$). This phenomenon is called concentration polarization and is described by the film theory [6,11]. By using the film layer model for concentration polarization, the concentration of the solutes near the membrane surface can be calculated as follows

$$C_{i,m} = C_{i,p} + \left(C_{i,f} - C_{i,p}\right)\exp\frac{J}{k} \tag{2}$$

and the real (intrinsic) rejection (R) is defined by the following equation

$$R = 1 - \frac{C_{i,p}}{C_{i,m}} \tag{3}$$

where $C_{i,m}$ is the concentration of solute i in the feed solution near the membrane surface, J is the permeate volume flux and k is the mass transfer coefficient in the polarization layer.

In Eq. (2), the mass transfer coefficient for the turbulent flow in tubular membranes (in our conditions, the Reynolds number is ≈17560) can be calculated from Eq. (4), i.e., the well-known Sherwood relationship with Deissler correlation [12]

$$Sh = 0.023 Re^{0.875} Sc^{0.25} \tag{4}$$

where the Reynolds (Re), Schmidt (Sc) and Sherwood (Sh) numbers are given by

$$Re = \frac{u\rho d_h}{\eta} \qquad Sc = \frac{\eta}{\rho D_{i,\infty}}, \text{ and} \qquad Sh = \frac{k d_h}{D_{i,\infty}} \tag{5}$$

where u is the fluid velocity in the channel whose hydraulic diameter is d_h (the diameter of the tubular membrane in our case), $D_{i,\infty}$ is the bulk diffusivity of solute i, and η and ρ are the dynamic viscosity and density of the aqueous solution, respectively.

DSPM Model

The extended description of DSPM model is provided with details elsewhere [5-7], and, therefore, only a brief description containing the main equations used in this work is given below.

The DSPM model is based on the extended Nerst–Planck equation (ENP) to describe the transport of a solute i through a porous membrane, modified to include steric effects for hindered transport in pores

$$j_i = -D_{i,p}\frac{dc_{i,m}}{dx} - z_i c_{i,m} D_{i,p}\frac{F}{RT}\frac{d\Psi}{dx} + K_{i,c} c_{i,m} J \tag{6}$$

with

$$D_{i,p} = 1 - K_{i,d} D_{i,\infty} \tag{7}$$

where j_i is the molar flux of solute i, $c_{i,m}$ is the concentration of solute i in the membrane, and the terms on the right side represent transport of solute i due to diffusion, electric field gradient and convection, respectively; $K_{i,d}$ and $K_{i,c}$ are

factors which account for the hindered diffusivity of the solute *i* in the liquid filled pores, which are reduced compared with their bulk values due to the particle-pore wall hydrodynamic interactions and also to the steric restrictions expressed by the solute *i* to pore size ratio $\lambda_i = r_{i,s}/r_p$ ($0 < \lambda_i < 1$).

When the uncharged solutes are considered, the electromigrative term in Eq. (6) is zero and, therefore, the solute is transported through the NF membrane only by convection and diffusion

$$j_i = -D_{i,p}\frac{dc_{i,m}}{dx} + K_{i,c}c_{i,m}J \tag{8}$$

By integration of Eq. (8) on the membrane thickness and for $c_{i,m}$ values between $C_{i,m}$ and $C_{i,p}$, the following expression is derived for the real (intrinsic) rejection [13]

$$R = 1 - \frac{C_{i,p}}{C_{i,m}} = 1 - \frac{\phi_i K_{i,c}}{1 - \left[\left(1 - \phi_i K_{i,c}\right)\exp(-Pe)\right]} \tag{9}$$

where the steric partitioning coefficient of solute *i* is $\phi_i = (1 - \lambda_i)^2$ and the Peclet number (*Pe*) is defined by Eq. (10) [13]

$$Pe = \frac{K_{i,c}J}{K_{i,d}D_{i,\infty}}\frac{\Delta x}{A_k} \tag{10}$$

The NF membranes can be modelled as a bundle of pores, and the hindrance factors $K_{i,d}$ and $K_{i,c}$ have different forms for different pore geometry (cylindrical or slit-like pores) [14,15]. The equations for hindrance factors for diffusion and convection in cylindrical pores derived by Decadilok and Deen [15], which were used in this work, are presented in Table I.

Thus, the rejection of uncharged solutes is determined only by steric effects, and the pore radius (r_p), and the thickness to porosity ratio ($\Delta x/A_k$) can be fitted from Eq. (9).

Moreover, the thickness to porosity ratio $\Delta x/A_k$ can be calculated from water flux measurements, by using the Hagen–Poiseuille equation [13]

$$J_w = L_p\Delta P = \frac{r_p^2}{8\eta(\Delta x/A_k)}\Delta P \tag{11}$$

where J_w is the pure water flux, L_p is the pure water permeability, ΔP is the transmembrane pressure and η is the solution viscosity.

By substituting the expression of $\Delta x/A_k$ provided by Eq. (11) in the expression of the Peclet number given by Eq. (10), an expression for the real rejection for each pore geometry which depends only on the pore radius is obtained from Eq. (9). By fitting the experimental retention data for all the

pressures with this equation which contains only one fitting parameter, the pore radius, r_p, can be calculated with high accuracy, and then the corresponding values of the thickness to porosity ratios ($\Delta x/A_k$) are computed from Eq. (11).

Table I Hindrance factors for diffusion and convection in cylindrical pores [15]

Convection	Diffusion
$K_{i,c} = \frac{1 + 3.867\lambda_i - 1.907\lambda_i^2 - 0.834\lambda_i^3}{1 + 1.867\lambda_i - 0.741\lambda_i^2}$	$K_{i,d} = \frac{H(\lambda_i)}{\phi_i}$; $H(\lambda_i) = 1 + \frac{9}{8}\lambda_i \ln\lambda_i - 1.56034\lambda_i + 0.528155\lambda_i^2 + 1.91521\lambda_i^3 - 2.81903\lambda_i^4 + 0.270788\lambda_i^5 + 1.10115\lambda_i^6 - 0.435933\lambda_i^7$

Spiegler–Kedem Model

The Spiegler–Kedem model [7] uses the irreversible thermodynamics for describing the transport of a single solute and solvent in NF and RO processes. This phenomenological model considers the membrane as a black box, and the solvent and solute transport is described by a sum of convective (due to the pressure gradient) and diffusive (due to the concentration difference existing at the membrane sides) fluxes. The transport coefficients of the Spiegler–Kedem model are: the water permeability (L_p), the solute permeability (ω) and reflection coefficient (σ). By applying linear relationships on a local level, the solvent flux, J_v, and the solute flux, j_i, are expressed by following equations

$$J_v = L_p(\Delta p - \sigma\Delta\pi) \tag{12}$$

$$j_i = \omega\Delta c_{i,m} + (1 - \sigma)J_v c_{i,m} \tag{13}$$

Assuming constant fluxes and constant coefficients σ and ω, Eq. (13) is integrated through the membrane thickness. This leads to the well-known Spiegler–Kedem equation, which relates the solute retention with the solvent volumetric flux and the solute permeability

$$R = \frac{\sigma(1 - F)}{1 - \sigma F} \text{ with } F = \exp\left(-\frac{1 - \sigma}{\omega}J_v\right) \tag{14}$$

The reflection coefficient is a measure of the ability of the membrane to separate solutes and has values between 0 and 1: σ = 0 means totally unselective membranes (no solute separation), and σ =1 means ideally semipermeable membrane (no solute transport) [7].

Teorell–Meyer–Sievers Model

The electrical properties of NF membranes can be described by Teorell–Meyer–Sievers (TMS) model [8,10], which considers only the electrostatic effects in order to explain the transport of charged solutes through NF membranes. This model assumes radially uniform distribution of fixed charges in a NF porous membrane, and it describes the electrical properties of the membranes by means of the effective fixed charge density of the membrane (ΦX).

For a salt solution of a 1-1 type electrolyte and a negative NF membrane, the TMS model equations which express reflection coefficient (σ) and solute permeability (ω) are given by the following equations

$$\sigma = 1 - \frac{2}{(2\alpha - 1)\xi + (\xi^2 + 4)^{1/2}} \tag{15}$$

$$\omega = D_s(1 - \sigma)\frac{A_k}{\Delta x} \tag{16}$$

where ξ is the parameter which expresses the electrostatic effects and is defined as the ratio of the fixed charge density of the membrane (X) to the concentration of the 1-1 electrolyte (c), $\xi = X/c$.

In Eqs (15) and (16), the transport number of the cation in the free solution (α) and the diffusivity of the 1-1 electrolyte (D_s) are calculated on the basis of the diffusion coefficients of the individual ions by using the relationships

$$\alpha = \frac{D_{+,\infty}}{D_{+,\infty} + D_{-,\infty}} \tag{17}$$

$$D_s = \frac{2D_{+,\infty}D_{-,\infty}}{D_{+,\infty} + D_{-,\infty}} \tag{18}$$

It is known that for most membranes the fixed charge density varies with the concentration of the electrolyte [8,16,17]. Therefore, in order to enable the interpretation of the relationship between the fixed charge density (X) and the concentration of the electrolyte (c), the effective fixed charge density of the membrane is used instead of X [8].

Experimental

Materials

AFC 80 membrane (PCI Membrane Systems) used in this study is a tubular thin-film composite NF membrane, consisting of an aromatic polyamide skin-layer on a polysulfone substrate. The membrane is capable of withstanding pressures up to 60 bars, temperatures below 70 °C and pH in 1.5-10.5 range.

All the reagents used were of analytical reagent grade or the highest purity available, and were used as received. The aqueous solutions were prepared by dissolving the reagents, i.e., sodium chloride NaCl, glycerol, ethanol, isopropyl alcohol, *t*-butyl alcohol (Penta Co., the Czech Republic) in highly demineralised water (conductivity < 1 μS cm^{-1}, pH 6.0 ± 0.1).

Permeation Experiments and Data Analysis

Nanofiltration experiments were performed by a cross-flow separation unit presented schematically in Fig. 1. The NF system was operated with a tubular MIC-RO 240 module manufactured by PCI Membrane Systems. The module was equipped with two tubular AFC 80 NF membranes of 1.25 cm internal diameter and 30 cm length, the effective membrane filtration area being 240 cm^2.

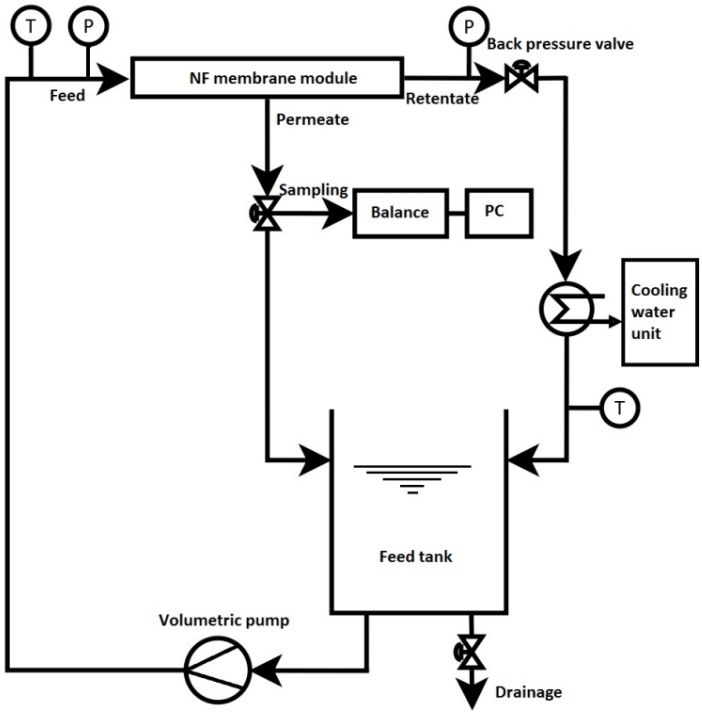

Fig. 1 Setup of nanofiltration experimental system

The experiments were performed at the constant temperature of the feed solution of 25 ± 0.5 °C and cross flow of 9 l min^{-1}, and the transmembrane pressure was varied in the range of 10-50 bar. The pure water flux (J_w) was measured at various transmembrane pressures in this range, and the membrane pure water permeability (L_p) was calculated. The value obtained for the pure water permeability is L_p = 1.45 ± 0.1 l m^{-2} h^{-1} bar^{-1} at 25 °C. The NF experiments were performed in the batch circulation mode, both permeate and retentate being returned to the feed tank in order to maintain a constant concentration in the feed. The permeate flux was determined by weighing, by using an electronic balance connected to a personal computer, and samples of permeate and feed were collected at each transmembrane pressure.

The structural characteristics of the membrane, i.e., the effective pore radius, r_p, and effective thickness to porosity ratio, $\Delta x/A_k$, were determined from the uncharged solutes rejection data. The experiments were performed by using 500 mg l^{-1} solutions of ethanol (MW = 46 g mol^{-1}), glycerol (MW = 92.1 g mol^{-1}), isopropyl alcohol (MW = 60 g mol^{-1}) and *t*-butyl alcohol (MW = 74 g mol^{-1}), at the natural pH of the demineralized water (6.0 ± 0.2). Their concentration in feed and permeate was determined by the total organic carbon (TOC) technique.

The membrane charge was estimated from permeation experiments of NaCl solutions with various concentrations in the range of 0.0025-0.05 M at pH 6.0 ± 0.2. The concentration of NaCl was measured with the sequential, radially viewed ICP (Inductively Coupled Plasma) atomic emission spectrometer INTEGRA XL 2 (GBC, Dandenong Australia).

In order to assure the reproducibility of the results, all the experiments were performed in duplicate. The reported values represent an average of two identical experiments, the relative standard deviation being up to 5 %.

As the membrane characteristics were determined by fitting with models, the quality of fitting was ascertained by calculating the coefficient of determination (R^2) and the non-linear parameter (χ^2) by using the following relationship [18]

$$\chi^2 = \sum \frac{\left(R_{exp} - R_{cal}\right)^2}{R_{cal}} \tag{19}$$

where R_{exp} and R_{cal} are the real rejections experimentally determined and calculated in accordance with the models, respectively. Very high values of R^2 and very small values of the parameter χ^2 indicate a good agreement between the experimental data and the theoretical model [18].

Results and Discussion

Determination of Membrane Structural Parameters

The NF experiments for structural characterization of AFC 80 membrane were performed by using 500 mg l^{-1} solutions of glycerol, ethanol, isopropyl alcohol and *t*-butyl alcohol. The pure water flux and the fluxes of the solutions used versus pressure are shown in Fig. 2.

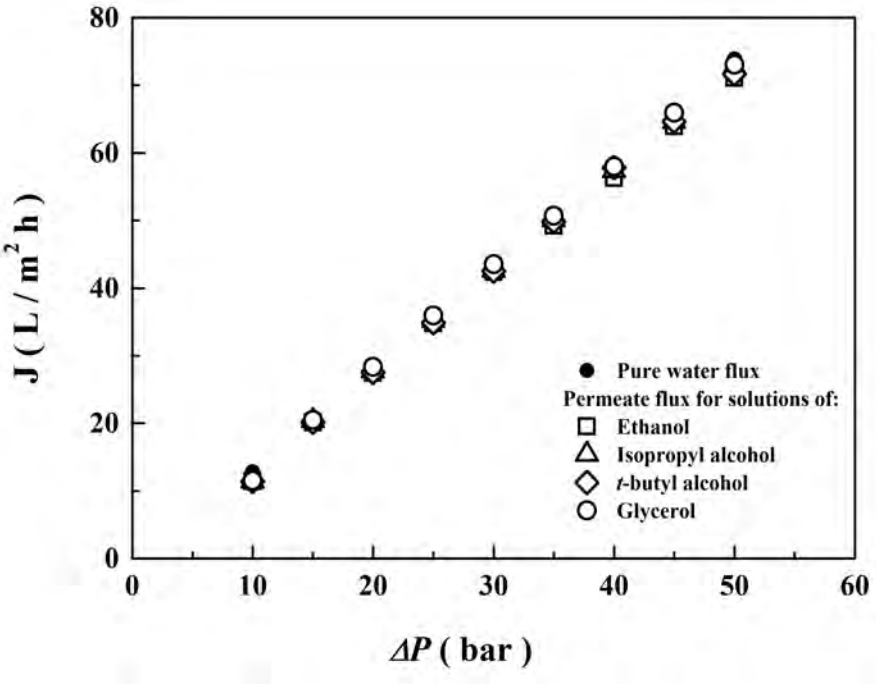

Fig. 2 Pure water flux and fluxes of the 500 mg l^{-1} solutions of glycerol, ethanol, isopropyl alcohol and *t*-butyl alcohol

Data in Fig. 2 show that the measured permeate flux vs pressure drop for the solutions of neutral solutes used are similar to the pure water flux, which indicates that the osmotic pressure of the solutions is negligible and the variations of the solutions properties (density, viscosity and diffusion coefficients) can be neglected, being considered identical with those of the pure water. This assumption is valid for such diluted solutions and, therefore, the calculations of the real rejections used for fitting with the DSPM model were performed using the water density and water viscosity ($\eta = 8.9\times10^{-4}$ Pa s).

The real rejections for 500 mg l^{-1} solutions of uncharged solutes are plotted in Fig. 3 as a function of the volume flux by the AFC 80 membrane. It can be observed that the higher the solute radius is, the higher the real rejection is (see the parameters of the solutes presented in Table II). The membrane parameters obtained by fitting r_p in Eq. (9) and then by calculating $\Delta x/A_k$ from Eq. (11) are also presented in Table II. Figure 3 and Table II show that Eq. (9) is fitting very

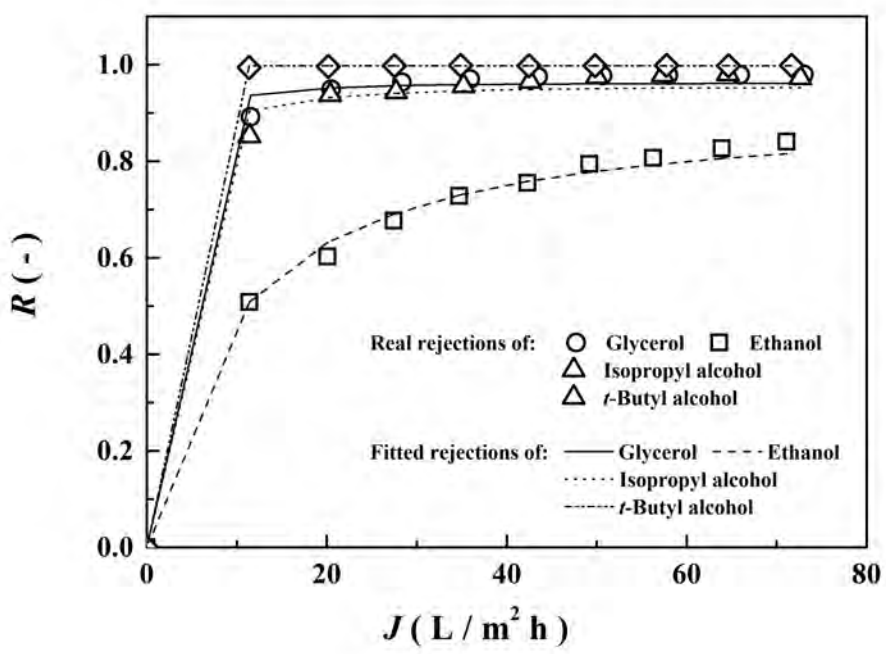

Fig. 3 Plot of experimental data for uncharged solute rejection by AFC 80 membrane and calculated rejections for fitting pore radius in Eq. (9)

Table II Characteristics of uncharged solutes and AFC 80 membrane parameters (r_p and $\Delta x/A_k$) calculated from their rejection by using DSPM model

Solute	Molecular weight	Diffusivity	Stokes radius	Membrane structural parameters		Quality of fitting r_p
	g mol^{-1}	10^{-9} m^2 s^{-1}	nm	r_p nm	$\Delta x/A_k$ μm	χ^2
Ethanol	46	1.24[a]	0.198[a]	0.287	2.88	3.60×10^{-3}
Isopropyl alcohol	60	1.02[a]	0.241[a]	0.3	3.13	6.03×10^{-3}
t-Butyl alcohol	74	0.88[a]	0.278[a]	0.293	3.00	1.64×10^{-5}
Glycerol	92.1	0.95[b]	0.258[b]	0.315	3.45	3.83×10^{-3}
				0.299 (average)	3.115 (average)	

[a] Data obtained from Ref. [8]
[b] Data obtained from Ref. [13]

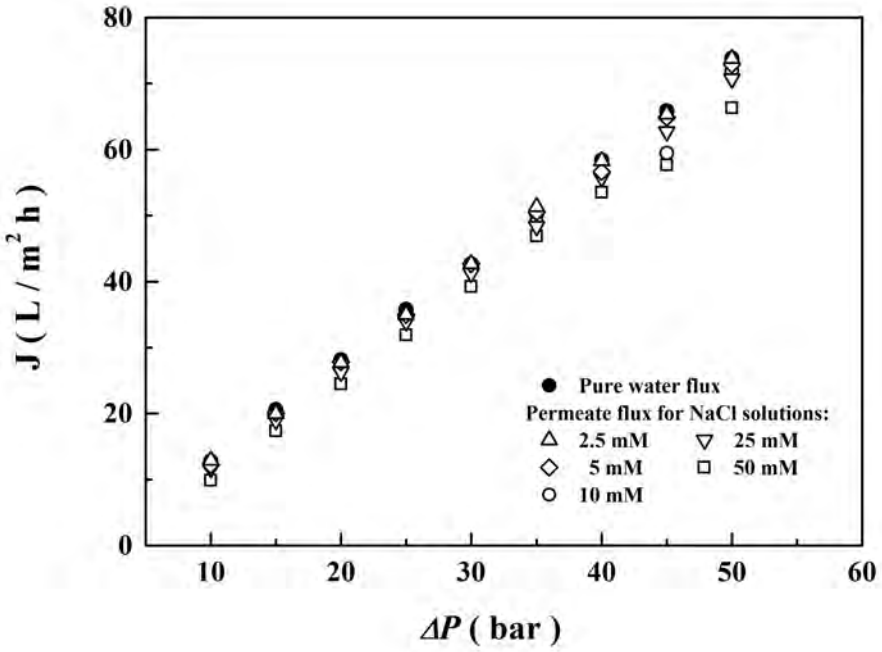

Fig. 4 Water flux and fluxes of NaCl solutions of various concentrations ranged from 2.5 to 50 mM.

well the experimental data for all the neutral solutes used as the values obtained for the non-linear parameter (χ^2) are very small. The pore radius and the thickness to porosity ratio obtained considering AFC 80 membrane modelled as a bundle of cylindrical pores are similar irrespective of the neutral solutes, and their average values calculated are $r_p = 0.299$ nm and $\Delta x/A_k = 3.115$ μm. The average value for pore radius presented in Table II indicates that AFC 80 membrane is a tight NF membrane close to the RO range, as it has very small pores. Other studies found similar pore radius about $r_p = 0.38 \pm 0.24$ nm and $r_p = 0.40 \pm 0.27$ nm [19].

Membrane Charge Density

The separation of charged solutes in NF is a combination of size exclusion and electrical interactions between the ions in the aqueous solution and the charged NF membranes. Therefore, the investigation of the membrane charge is an important step in order to understand and to predict the NF processess. The membrane charge is determined by the chemical structure of the membrane material, and it occurs from dissociations of functional groups of membrane material or due to adsorption of charged or polarizable solutes from the solution. AFC 80 membrane used has a polyamide top layer containing ammonium ($-NH_3^+$) and carboxyl (–COOH) groups, and it has an isoelectric point at pH about 3.6 in KCl solution [20]. Thus, at pH < IEP the membrane is positively charged as the carboxyl groups are undissociated and the amine groups are protonated, and at pH > IEP the membrane has a negative charge as the carboxyl groups are dissociated.

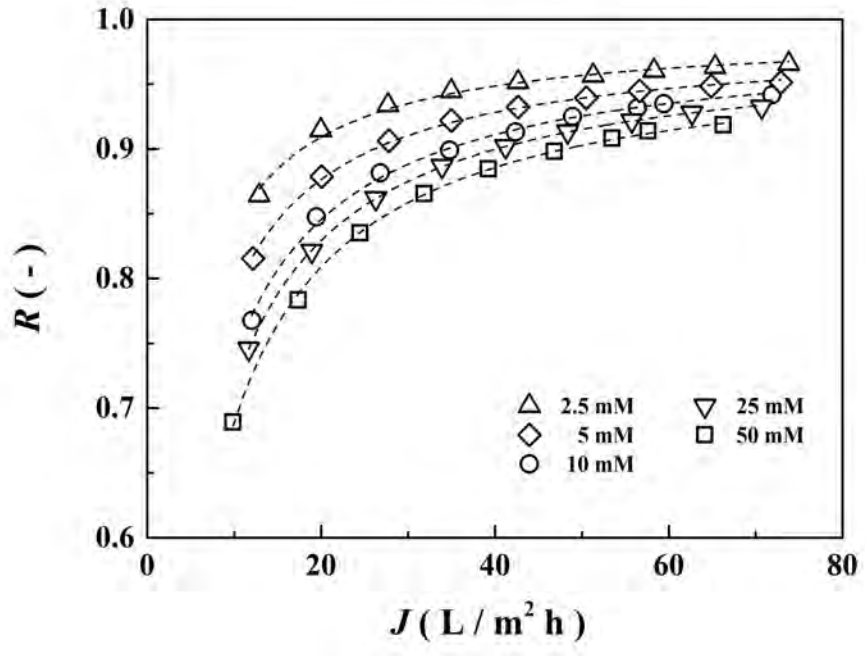

Fig. 5 Rejection of NaCl by AFC 80 membrane as function of volume flux for feed solutions with various concentrations ranging from 2.5 to 50 mM. Experimental data (points) were fitted by Spiegler–Kedem model equation (dashed lines)

In order to calculate the membrane charge, the separation experiments of NaCl solutions with the concentration in the range of 2.5-50 mM were performed. The water flux and the permeate fluxes versus applied pressure for the salt solutions used presented in Fig. 4 show that the permeate flux is slightly decreasing with increasing the concentration of NaCl solution as a consequence of the increase in osmotic pressure.

Figure 5 shows the dependence of the real rejection as a function of the permeate volume flux for NaCl solutions with various concentrations. The salt diffusivity $D_s = 1.61\times10^{-9}$ m^2 s^{-1} used to compute the real salt rejections was calculated by using Eq. (18) on the basis of the diffusion coefficients of the individual ions: $D_{\infty,Na^+} = 1.333\times10^{-9}$ m^2 s^{-1} and $D_{\infty,Cl^-} = 2.031\times10^{-9}$ m^2 s^{-1} [19].

As presented in Fig. 5, the solute rejection decreases with an increasing NaCl concentration in the aqueous solution, and an increase in the applied pressure significantly increased the solute removal for all NaCl concentrations investigated. Salt retentions were fitted with the Spiegler–Kedem model (dashed lines in Fig. 5), and the values of the parameters of the model obtained are given in Table III. The values of the effective fixed charge density (ΦX) calculated from Eq. (15) on the basis of these reflection coefficients are depicted in Fig. 6 together with the dependence of the reflection coefficient on the concentration of NaCl solutions.

Data in Fig. 5 and Fig. 6 and the values of the non-linear parameter χ^2 in Table III show that the Spiegler–Kedem model describes very well the experi-

Table III Reflection coefficients (σ) and solute permeabilities (ω) obtained by fitting experimental data of NaCl rejection with Spiegler–Kedem model

NaCl concentration	Spiegler–Kedem model parameters		Effective fixed charge density	Quality of fitting
mM	σ	ω l m^{-2} h^{-1}	$-\Phi X$ mM	χ^2
2.5	0.984	1.807	402.083	1.037×10^{-5}
5	0.976	2.5	552.520	5.165×10^{-6}
10	0.977	3.34	1032.089	3.557×10^{-7}
25	0.97	3.672	2035.848	2.486×10^{-6}
50	0.961	4.146	3511.306	1.071×10^{-7}

mental rejection data for all the NaCl concentrations investigated. The reflection coefficient (σ) decreases and the solute permeability (ω) increases by increasing salt concentration in feed solution, which stands in an agreement with the gradually decreasing rejection when increasing the concentrations of the solutions obtained experimentally and depicted in Fig. 5. Thus, it can be assumed that the Spiegler–Kedem model gives a good description of the experimental results of NaCl rejection.

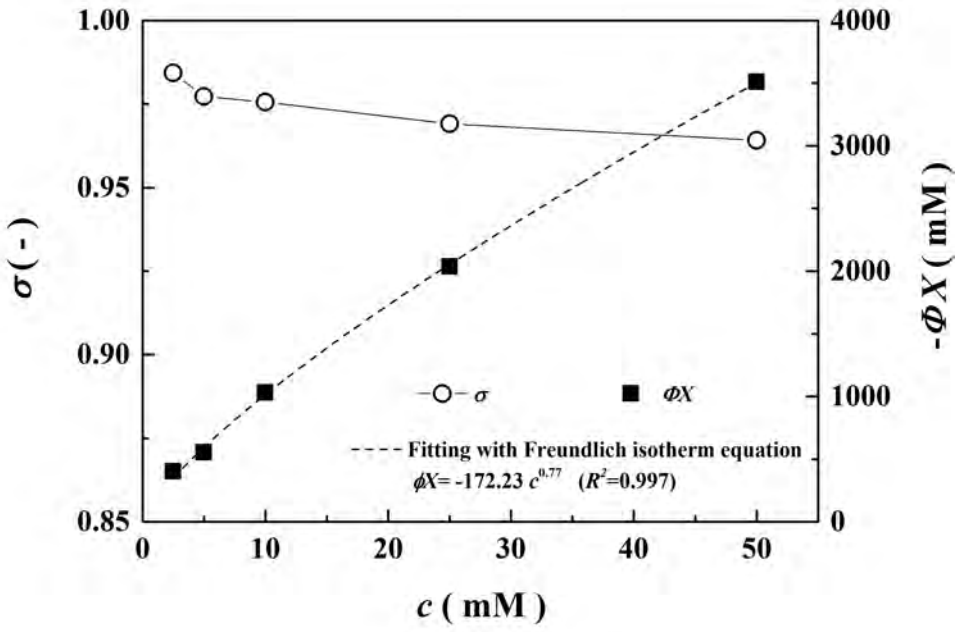

Fig. 6 Reflection coefficient and effective fixed charge density of AFC 80 membrane as function of NaCl concentration in feed. Effective charge density values vs concentration were fitted with Freundlich isotherm equation (dashed line)

Figure 6 shows the dependence of the effective fixed charge density (ΦX) of the AFC 80 membrane calculated from Eq. (15) on the NaCl concentration in the solution. It can be observed that the membrane charge is strongly dependent on the concentration of the solution with which the membrane is in contact; the membrane negative charge is increasing monotonically when the NaCl concentration in the aqueous solution increases. This behaviour was observed by other authors, and it can be attributed to the adsorption of ions from solution on the membrane surface [3,5,8,16]. In our case, the increase in the negative membrane charge can be determined by the adsorption of chloride ions on the membrane. Indeed, Fig. 6 shows that the data obtained for the effective charge density at different concentrations of the electrolyte solution are consistent with an adsorption process as they are fitted quite well by Freundlich isotherm equation. Similar dependencies of the membrane charge density were reported by other authors for similar NF membranes [3,5,8,16]

Conclusion

In the present study, an overall characterization of the polyamide thin-film composite NF membrane, AFC 80, was performed by using modelling the rejection experiments. The structural and electrical properties of the membrane were expressed in terms of three parameters, i.e., effective pore radius (r_p), thickness to porosity ratio ($\Delta x/A_k$) and effective fixed charge density (ΦX). Donnan steric partitioning pore model (DSPM) is useful for structural characterization, and it reveals that AFC 80 is a tight NF membrane which possesses pores with radius about 0.3 nm. Based on the Spiegler–Kedem model and on Teorell–Meyer–Sievers (TMS) model, the charge density of the AFC 80 membrane was evaluated from rejection experiments of NaCl solutions of various concentrations. The charge density of the membrane was found to be dependent on the concentration of the electrolyte solution, namely it increases with increasing the solution concentration as predicted by the Freundlich isotherm adsorption equation. This suggests that ions from the solution are adsorbed on the membrane surface and thus increase their negative charge.

Acknowledgement

Cristina-Veronica Gherasim gratefully acknowledges the financial support for the research of the The Ministry of Education, Youth and Sports of the Czech Republic, Project CZ.1.07/2.3.00/30.0021 "Strengthening of Research and Development Teams at the University of Pardubice".

Symbols

A_k membrane porosity
$C_{i,f}$ concentration of solute *i* in feed solution, mol m^{-3}
$C_{i,m}$ concentration of solute *i* in feed solution at membrane surface, mol m^{-3}
$C_{i,p}$ concentration of solute *i* in permeate solution, mol m^{-3}
$c_{i,m}$ concentration of solute *i* in membrane, mol m^{-3}
$D_{i,\infty}$ bulk diffusivity of solute *i*, $m^2\ s^{-1}$
d_h hydraulic diameter, m
D_s effective diffusivity of salt, $m^2\ s^{-1}$
J permeate volume flux, $m^3\ m^{-2}\ s^{-1}$
j_i molar flux of solute *i*, mol $m^{-2}\ s^{-1}$
J_v solvent volume flux, $m^3\ m^{-2}\ s^{-1}$
J_w pure water flux, $m^3\ m^{-2}\ s^{-1}$
k mass transfer coefficient in polarization layer, m s^{-1}
$K_{i,c}$ hindrance factor for convection
$K_{i,d}$ hindrance factor for diffusion
L_p pure water permeability, m s^{-1} Pa^{-1}
p pressure, Pa
$r_{i,s}$ Stokes radius of component *i*, m
r_p pore radius, m
Pe Peclet number
R real (intrinsic) rejection
R_o observed rejection
Re Reynolds number
Sc Schmidt number
Sh Sherwood number
T absolute temperature, K
u fluid velocity in channel, m s^{-1}
x distance in membrane, m
X fixed charge density, mol m^{-3}
z_i valence of solute *i*

Greek symbols

α transport number of cation in solution
ΔP transmembrane pressure, Pa
$\Delta\pi$ osmotic pressure, Pa
η dynamic viscosity, Pa s
ρ density, kg m^{-3}
ϕ_i steric partitioning coefficient of solute *i*
ΦX effective fixed charge density, mol m^{-3}
λ_i solute *i* to pore size ratio

ω solute permeability, m s^{-1}
σ reflection coefficient
ζ ratio of fixed charge density to salt concentration

References

[1] Schäfer A.I., Fane A.G., Waite T.D. (Eds.): *Nanofiltration: Principles and Applications,* Elsevier, Oxford, UK, 2005.
[2] Linde K., Jonsson A. S.: Desalination **103**, 223 (1995).
[3] Schaep J., Vandecasteele C., Mohammad A. W., Bowen W. R.: Sep. Sci. Technol. **34**, 3009 (1999).
[4] Mulder M., *Basic principles of membrane technology*, 2nd ed., Kluwer Academic Publishers, Dordrecht, 1996.
[5] Bowen W.R., Mukhtar H.: J. Membr. Sci. **112**, 263 (1996).
[6] Bowen W.R., Mohammad A. W., Hilal N.: J. Membr. Sci. **126**, 91 (1997).
[7] Spiegler K., Kedem O.: Desalination **1**, 311 (1966).
[8] Wang X.L., Tsuru T., Togoh M., Nakao S., Kimura S.: J. Chem. Eng. Jpn. **28**, 186 (1995).
[9] Szymczyk A., Fievet P.: J. Membr. Sci. **252**, 77 (2005).
[10] Hoffer E., Kedem O.: Desalination **2**, 25 (1967).
[11] Zydney A.L.: J. Membr. Sci. **130**, 275 (1997).
[12] Deissler R.G.: *Analysis of turbulent heat transfer, mass transfer and friction in smooth tubes at high Prandtl and Schmidt numbers*, National Advisory Committee for Aeronautics (NACA), Rep 1210, 1955.
[13] Cavaco Morao A.I., Szymczyk A., Fievet P., Brites Alves A.M.: J. Membr. Sci. **322**, 320 (2008).
[14] Deen W.M.: AIChE J. **33**, 1409 (1987).
[15] Dechadilok P., Deen W.M.: Ind. Eng. Chem. Res. **45**, 6953 (2006).
[16] Kobatake Y., Takeguchi N., Toyoshima Y., Fujita H.: J. Phys. Chem. **69**, 3981 (1965).
[17] Gherasim C. V., Mikulášek P.: Desalination http://dx.doi.org/10.1016/ j.desal.2013.11.012, (2013).
[18] Foo K.Y., Hameed B.H.: Chem. Eng. J. **156**, 2 (2010).
[19] Otero J.A., Lena G., Colina J.M., Pradanos P., Tejerina F., Hernandez A.: J. Membr. Sci. **279**, 410 (2006).
[20] Gherasim C. V., Cuhorka J., Mikulášek P.: J. Membr. Sci. **436**, 132 (2013).